UNIVERSITY OF CALIFORNIA, MERCED

# Implementation of thermodynamically efficient collectors for medium high temperature applications

A Dissertation submitted in partial satisfaction of the requirements

for the degree of PhD

in

Environmental Systems

by

Lun Jiang

Committee in charge:

Professor Gerardo Diaz, Chair

Professor Roland Winston

Professor Yanbao Ma

Professor Michael Modest

Fall 2014

Dissertation of Lun Jiang

is approved by:

---

Professor Gerado Diaz(Chair)

---

Professor Roland Winston

---

Professor Yanbao Ma

---

Professor Michael Modest

# Contents

## List of Symbols

$A_{col}$ solar collector aperture area ($m^2$)

$c_p$ specific heat capacity (J/kg-K)

$I$ solar irradiance ($W/m^2$)

$C$ concentration ratio

$\dot{m}$ mass flow rate (kg/s)

$Q$ thermal power (W)

$q$ heat flux($W/m^2$)

$T$ temperature (° C)

$W$ work (W)

$U_L$ heat transfer coefficient ($W/m^2$)

$V$ Voltage (volt)

$I$ Current (ampere)

$P_{12}$ Probability of the radiative heat transfer from 1 to 2. This is the view factor under certain geometry of ideal mirror.

Greek letters

$\eta$ efficiency

$\Delta$ delta

$\tau$ transmission of the collector cover or glass tube

$\alpha$ absorption of the absorber

$\theta_a$ half acceptance angle

$\epsilon$ emissivity

$\sigma$ Stefan's Constant

Subscripts

| | |
|---|---|
| col | collectors |
| aper | aperture |
| loss | collector heat loss |
| radiLoss | radiative loss |
| abs | absorbed heat for the collector |
| m | medium temperature of the working fluid |
| useful | heat extracted from the collector |
| cal | calorimeter |
| tot | total irradiance |
| acc | half acceptance angle |

Abbreviations

IAM - Incident Angle Modifier

DNI - Direct Normal Irradiance

EW - East / West

NS - North / South

XCPC - eXternal Compound Parabolic Concentrator

ICPC - Integrated Compound Parabolic Concentrator

kW - Kilowatt

kWh - Kilowatt Hour

PSP - Precision Spectral Pyranometer

NIPS - Normal Incidence Pyrheliometer

PTC - Parabolic trough concentrator

UC - University of California

Ch - Selective coating from Chinese supplier, typically cermet coatings

## 1. Introduction

Solar thermal collectors have had a long history since ancient Greek time, when people started to heat up hot water in a black painted box under the sun. The modern solar thermal collectors, although still using the same underlying principles of physics, are altogether different from what it used to be. Last 40 years of R&D for new materials, optics, and vacuum technology have enabled multiple generations of successful solar thermal collectors to be adopted into wide spread usage around the world. However, the story of such collectors is not ended. Facing unprecedented pressure from climate change, reducing the GHG(Green House Gas) from conventional energy sources creates an opportunity for the next generation of such collectors. New requirements for the next generation of solar thermal collectors are, for example, improved efficiency, higher working temperature, simplistic design, cost effective for mass production, integrated design, and ready to work with other types of energy.

In this thesis, an effort is made to observe the underlying principles for the improvements of such collectors, specifically, the optical design and the absorber shape design for vacuum receivers. A number of solar thermal collectors, with optimized optics, heat transfer and production procedure are tried, examined and analyzed. The different possible parameters of the design are often tried out in an early simulation stage, followed by a fabrication of the prototype. Eventually an experimental characterization result is produced to both prove and measure the efficiency of a small scale implementation. Depending on the result, an iterative process is repeated with the steps above to perfect the prototype, until it is ready for commercialization. Through example of such iterations, this thesis will showcase and summarize the lessons that have been learned from both the theoretical and the engineering discussions.

## 1.1 Backgrounds for solar thermal collectors

Application temperature ranges:

Solar thermal application has a wide range of temperature. It can be roughly divided into the following three categories.

a. Low temperature application. (<100 °C)

   The application of this range includes space heating, domestic hot water, and is the currently most developed market of solar thermal. It is characterized with lower pressure for heat transfer fluid. Water is generally used carry out the heat from the collector, some application, such as space heating, allows air to be circulated at the sacrifice of heat transfer efficiency. Low pressure enables the collector design to have less requirement for pressurization and therefore reduces the production cost of collector to minimum.

b. Medium high temperature application. (100 °C to 250 °C)

   Many industrial processing heat processes are accounted for in this temperature range, and a significant market is the double effect absorption chiller which allows space cooling with solar thermal source. Boiler preheating and steam generation can also be widely adopted with solar thermal as an alternative to fossil energy source. This range is currently underdeveloped, unexplored, and pioneered with very few large scale projects compared to the highly mature low temperature solar applications. The technology in this temperature range finds itself in a dilemma of being inaccessible, temperature wise, for low temperature collectors. It is also unavailable for higher temperature arrays to be utilized because of size and cost issues.

c. High temperature application. (300 °C and above)

Very few applications using solar thermal exist between 200°C and 300°C, however, the typical temperature for electricity production is above 300°C. At this temperature the steam generated by the solar array can efficiently drive a turbine. (Solar towers can operate above 600°C.) The advantages of using solar thermal for power production are its capabilities of storage and the integration with the existing gas/coal fired power plant, which is readily available. Its disadvantage is not being able to compete with currently underpriced polycrystalline silicon solar panels.

## 1.2 Tracking and non-tracking

Solar thermal technologies can be categorized into two divisions: tracking and non-tracking. Tracking systems are primarily meant for the high temperature range applications, such as power generation and industrial processing heat. They concentrate direct sunlight onto a receiver which has a working medium that carries the thermal energy to the load of the aforementioned applications. Non-tracking systems have primarily been used for the low temperature applications such as residential water heating. With evacuated tubes and the development of nonimaging optics, new solar thermal concentrators have been developed that are non-tracking. However, they are capable of producing heat in the medium temperature range and possibly the high temperature range.

## 1.3 Nonimaging optics in solar thermal applications

Nonimaging optics makes the limit of the geometric concentration calculable. Therefore the solar energy industry has been benefitting from this theory and its design since the 1980's. However, the effort of the industry to catch up with an implementation of the designs of this theory has not achieved any popular products with affordable cost. The recent revisited

attention towards renewable energy under the pressure of climate changes has brought a lot of attention to the possibility of constructing affordable medium and high temperature solar thermal collectors. As always, the unique capability of nonimaging optics being able to provide an answer to both the question of geometric concentration limit and corresponding design methods is important to be adapted to this new, ever evolving technological/economical context of solar energy. It is also required by industry for the designs to be flexible and sometimes even compromised for the limitation of material, labor and installation cost. UC Solar has the capability to both design and prototype this kind of non-tracking concentrators within the context of an evacuated tube.

The thesis work includes the design, prototyping, testing and reiteration of the prototyping of a solar thermal collector. The goal of such a thermal collector is to achieve 60% efficiency at 200°C and functions up to 275°C with non-tracking solar concentration integrated with the evacuated tubes. The material cost of the collector is targeted at $5 per square foot and the module cost at $10 per square foot. This goal will produce a ground breaking efficiency improvement for the solar thermal products within the temperature range of 100°C - 200°C, with a similar or lower cost of production.

## 1.4 Market for mid-temperature solar thermal collectors

Solar thermal application escapes our general public attention. The current low temperature (below 100 °C) domestic market is mainly in European countries like Germany, and in China, with very limited public awareness in other countries. However, in year 2010, the newly installed solar thermal collectors accounted for $38GW_{thermal}$ heat generation worldwide [1]. Compared to the $38GW_{thermal}$ heat generation, the world wide newly installed solar PV only generated $35GW_{electricity}$ in the year 2011. Despite the current

success in domestic solar thermal applications, the solar thermal industrial processing application remains at the stage of demonstration projects. The task 49 of the IEA SHC program points out that 28% of the industrial energy demand is in thermal, among which 30% is below 100 °C, and 57% is below 400°C ([1], Table 1.). The underwhelming development of solar thermal application in industry is mainly due to the lack of new technology and the long term testing of stable products. The current existing domestic water heaters cannot satisfy the requirement of the temperature and the pressure required for general industrial steam production.

Within the temperature range of 140 °C to 180 °C, solar thermal collectors can be also used for space heating and cooling with a double effect absorption chiller (non-electric chiller). There are only about 600 demonstration projects for solar cooling worldwide. Most of which still use single effect absorption chillers due to the unavailability of the medium temperature solar collectors.

Almost all of the major low temperature solar thermal collector producers are actively seeking for technologies that can enable a pressurized system to reach the medium temperature range. Recently the solar market of this temperature range started attract more attention. Enterprises start to pay attention to both developing the products and the testing methods. Companies such as Tinox, one of the biggest selectively coated absorber producers in the world, is showing products exclusively developed for 200 °C in their exhibitions. SPF, which is the testing center for solar thermal collectors in Europe, is renovating their testing platform for medium temperature solar collectors.

## 2 Thermodynamically efficient optics

The heat transfer of a solar collector involves three heat sinks: the sun, the working fluid, and the ambience. The energy exchange between the solar resource and the working fluid is the useful energy to be extracted out of a collector. A thermodynamically efficient solar collector is required to exchange energy only between the sun and the working fluid. Optically, this is equivalent to a reverse ray tracing in such a way that any virtual rays coming from the absorber will be arriving only at the source, e.g. the sun. There would be no radiative heat transfer from the absorber to the ambience[2].

## 2.1 Efficient stationary solar collectors

The efficiency of a solar collector is simply the energy extracted by the solar collector divided by the radiation energy received by the collector. The useful energy in this case is limited by the optically absorbed energy and the heat dissipation into the environment.

$$Q_{useful} = Q_{abs} - Q_{loss} \tag{1}$$

$$Q_{loss} = Q_{radiLoss} + Q_{cond} + Q_{conv} \tag{2}$$

$$\eta_{collector} = \frac{Q_{useful}}{Q_{col}} < 1 \tag{3}$$

$$Q_{col} = I_{Tot} A_{aper}, \qquad Q_{abs} = Q_{col} \tau\alpha \cdot (IAM) \tag{4}$$

Here the heat loss from the collector to the ambience is $Q_{loss}$, heat loss consists of radiation, convection and conduction. The conductive and convective loss of the collector can be approximated with first and second order polynomial fitting[3][4][5] and analyzed through a model of thermal resistance[6].

The conduction and convection heat loss are typically approximated by

$$Q_{cond} + Q_{conv} = A_{abs} U_L(T_m) \cdot (T_m - T_{amb}) \tag{5}$$

Here the overall loss coefficient $U_L$ can be treated as a constant at lower temperatures, according to the collector type. But with the free convection and the change of the thermal properties of the collector material, one would need to introduce higher orders for the $U_L$ (first order typically) to describe the heat transfer coefficient.

$$U_L(T_m) = c_0 + c_1 T_m + \cdots \tag{6}$$

Any order increase in $U_L$ from equation (6) will result in another order increase in equation (5).

Radiative heat loss plays a more important role in higher temperature solar collector designs. It increases based on the fourth order of the working temperature according to Stefan-Boltzmann law.

$$q_{radiLoss} = \sigma\epsilon({T_m}^4 - {T_{amb}}^4) \tag{7}$$

$$Q_{radiLoss} = \sigma\epsilon A_{abs}({T_m}^4 - {T_{amb}}^4) \tag{8}$$

To summarize EQ (1) through (6),

$$Q_{radiLoss} = \sigma\epsilon A_{abs}({T_m}^4 - {T_{amb}}^4) \tag{9}$$

$$\eta_{col} = \frac{I_{tot} A_{aper} \tau\alpha \cdot (IAM) - (c_0 + c_1 T_m) A_{abs} \cdot (T_m - T_{amb}) - \sigma\epsilon A_{abs}({T_m}^4 - {T_{amb}}^4)}{I_{tot} A_{aper}} \tag{10}$$

$$\eta_{col} = \tau\alpha \cdot (IAM) - \frac{(c_0 + c_1 T_m) A_{abs} \cdot (T_m - T_{amb}) + \sigma\epsilon A_{abs}({T_m}^4 - {T_{amb}}^4)}{I_{tot} A_{aper}} \tag{11}$$

$$\eta_{col} = \tau\alpha \cdot (IAM) - \frac{(c_0 + c_1 T_m) \cdot (T_m - T_{amb}) + \sigma\epsilon({T_m}^4 - {T_{amb}}^4)}{I_{tot} C} \tag{12}$$

From equation (12), the total irradiance is a limited resource. Transmission and absorption values are determined by the material utilized. Therefore optically one can only change the incident angle modifier ($IAM$) and the concentration ratio ($C$) to affect the efficiency of the collector; this explains the requirement for concentration ratio in the higher temperature solar thermal applications as shown in Fig.1 [7]

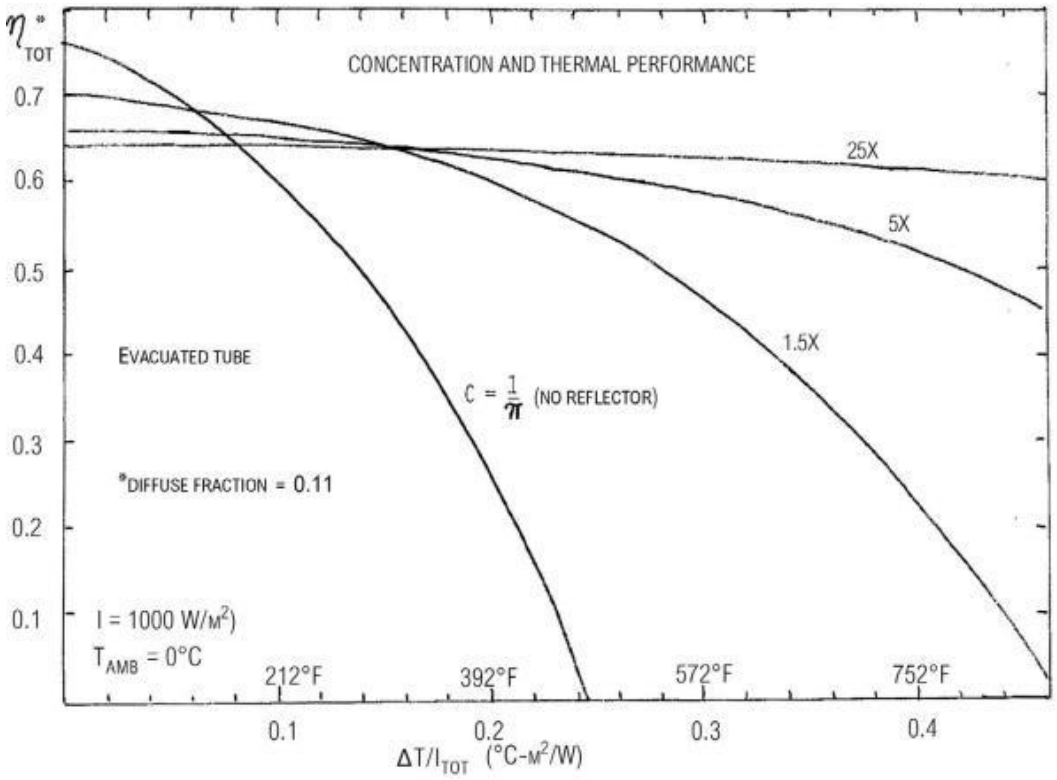


Fig.1. Efficiency of the solar thermal collector according to temperature and concentration ratio.

The concentration ratio is limited by étendue conservation, or the second law of thermodynamics[2] [8], which states that:

$$C_{max} = 1/\sin\theta_{acc}$$

,where $C_{max}$is the maximum concentration ratio and $\theta_{acc}$is the half acceptance angle of the collector. The concentration described here is one dimensional or for an extruded absorber.

Equipped with this theory, we can calculate the non-tracking and stationary concentrator limit according to the seasonal change of the sun:

$$C_{max} = \frac{1}{\sin(35.5°)} = 1.722$$

This concentration ratio is able to increase the working temperature of a 120°C solar collector to 165°C with exactly the same radiative heat loss. Here the collector is positioned east-west with at least 7 hours of solar collection.[9]

Given the working temperature, in order to achieve higher efficiency, the collector design seeks to lower the emissivity $\epsilon$ and increase the concentration ratio $C$. With the current technology, by engineering the surface property of the absorber, the $\epsilon$ for $T_m$ up to 350˚C has achieved values less than 6%. The heat loss per area $Q_{radiLoss}$ using such a material is still $500W/m^2$ at this temperature. This is 50% loss compared to the $1000W/m^2$ solar irradiance for standard characterizing condition for solar collectors. This is unacceptable for an efficient solar collector design. Therefore the additional concentration ratio enabled by nonimaging optics is important in promoting the efficiency of a solar collector, if it is working at medium high temperature. This has also proven to be true for the secondary receiver design.(Fig.2)

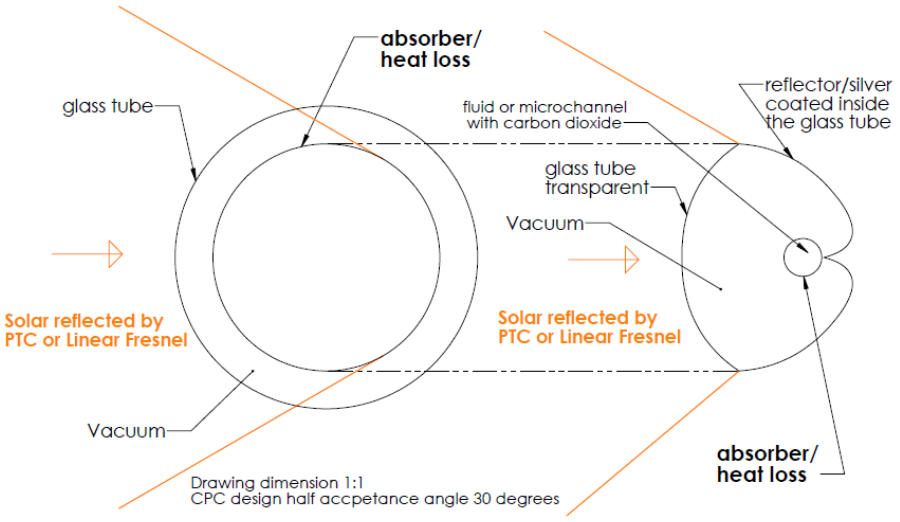


Fig. 2. A comparison of the solar absorber size for evacuated tubes under 30 degrees half acceptance angle.

2.2 The improvement of Optics under thermodynamic limit assumption

Asymmetric design for Compound Elliptical Concentrators(CEC) is one example of such an improvement. The conventional CPC assumes the edge ray to be symmetric. A. Rabl suggested an asymmetrical CPC design, and also a symmetric design of CEC for a finite source. In this thesis we expand the method to an asymmetric finite sources, the proof of it is provided as the following.

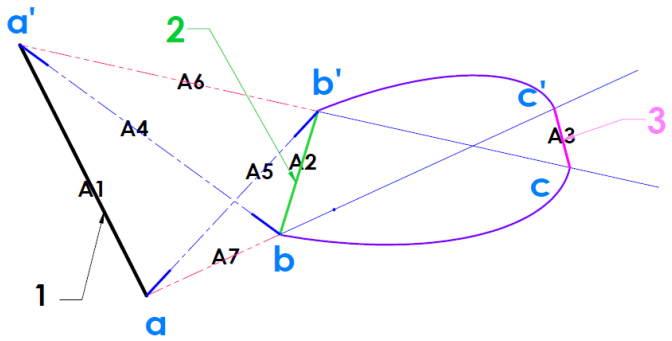


Fig. 3. The diagram for asymmetric CEC generated from finite source.

1. Choose source 1

2. Choose absorber 3

3. Connect ac', a'c

4. Use a, c as foci, starting at c' and draw the elliptical profile, crossing the a'c at b'

5. Repeat above for a', c'

6. $cc' + a'c = a'b + bc' and\ cc' + ac' = ab' + b'c$

7. Adding the two above together. Because $a'c - b'c = a'b' and\ ac' - bc' = ab$

$$2cc' = a'b + ab' - (a'b' + ab)$$

8. $P_{21}A_2 = \frac{1}{2}\left[\sum long\ strings - \sum short\ strings\right] = 2cc' = A_3$

9. The Hottel strings automatically satisfied the thermodynamic 2nd law[10].

2.3 Symmetric design for any shape of convex absorber.

A program based on the inspiration of flow line design[11] is implemented to produce nonimaging concentrator for any convex shape. The program can be described in the following sequences.

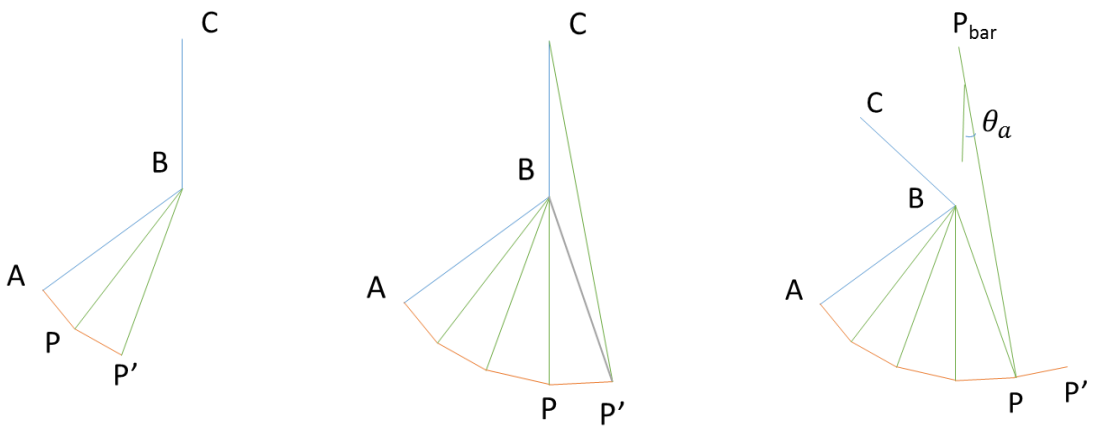


Fig.4 The process of forming the involution edge ray for any convex absorber using CPC design.

a) Refer to Fig.4. left ABC is part of the discretized absorber, the involution starts at point A, and has arrived at point P. The calculation of next point P' is performed by having PP' reflecting the ray BP back to point B. The angle $\angle PBP'$should be minimized according to the accuracy of the program. The fine tuning of this accuracy is crucial for the fidelity of the curve.

b) As shown in Fig.4. middle, after certain number of iterations, the point P' will cross over the tangent line of the absorber, CB, in this case a quick cross product of CB, BP' can be checked to determine if the point B needs to be updated to the point C. This step is repeated until P'C can no longer be found under the half acceptance angle.

c) As shown in Fig.4. right, the line BC can be beyond the acceptance angle, a check of the cross product of $PP_{bar}$ and BC can be checked. Under this condition the ray BP should be reflected back to point $P_{bar}$.

d) The process is repeated until the truncation ratio is reached for the aperture, or the edge of the curve is vertical. As shown in Fig.5, this is the result used in our pentagon shape absorber prototype.

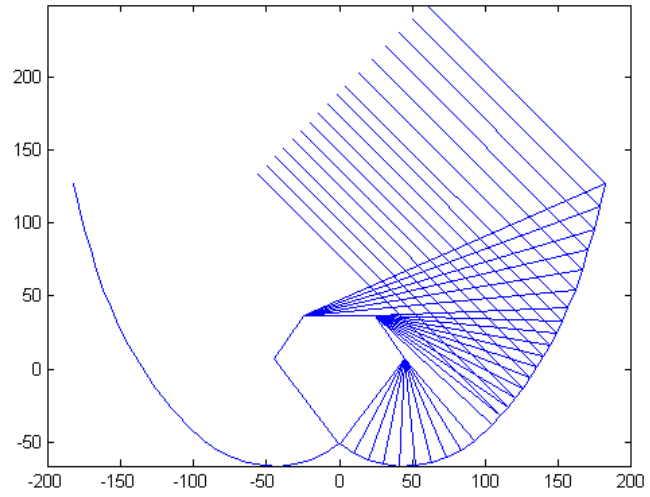


Fig.5 The involute edge ray of a pentagon absorber produced by the program in low accuracy.(in mm).

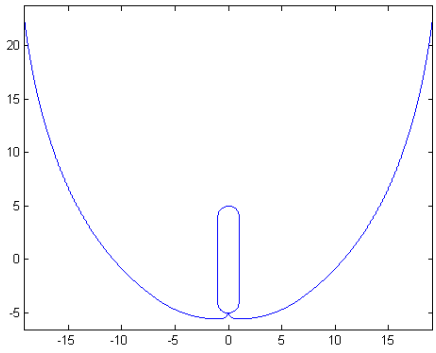


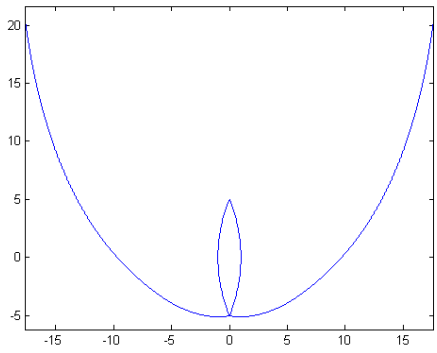

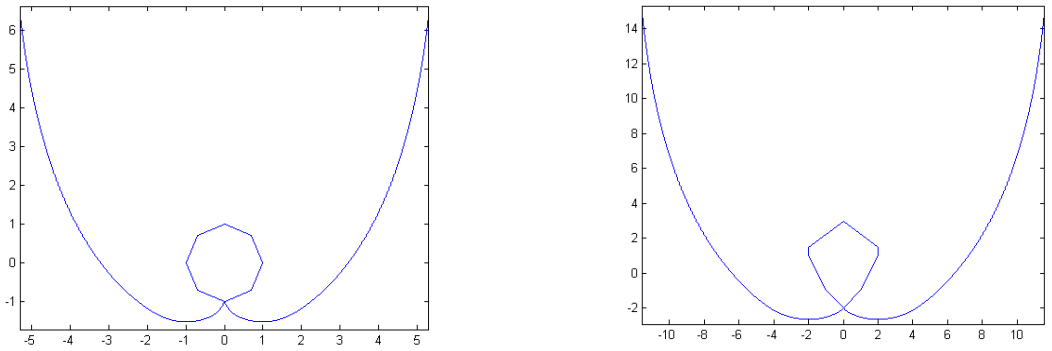

Fig.6 The result for arbitrary convex absorbers.

## 3 The prototyping of the next generation of non-tracking solar thermal collector

### 3.1 Fabrication of the next gen XCPC

Pushing forward in the XCPC array involves the customization of collector using proper selective coating as the absorber. A comparison was performed among several commercially available selective coatings. The experiment is conducted as the following:

A. All selectively coated absorbers came as flat samples, coated on aluminum or copper.

B. The samples are used in making counter flow metal glass vacuum tubes[12][13].

C. They are tested side by side on the same day, under the same solar condition. The temperature rise were observed and recorded every few minutes.

| Time | Tilted Global Irradiance | JinHeng(Al) | | | TuoMa(Al) | | | Tinox back to back | | Tinox(Cu) | | Tinox(Al) | | Alanod(sunselect,Cu) | | Yin(Cu) | | Yin(Al) | |
|---|---|---|---|---|---|---|---|---|---|---|---|---|---|---|---|---|---|---|---|
| | | 1 | 2 | 3 | 1 | 2 | 3 | Cu | Al | 1 | 2 | 1 | 2 | 1 | 2 | 1 | 2 | 1 | 2 |
| 0min | 860 | 71 | 75 | 77 | 77 | 72 | 67 | 128 | 148 | 88 | 92 | 60 | 70 | 85 | 89 | 136 | 134 | 88 | 102 |
| 5min | 793 | 163 | 159 | 164 | 146 | 138 | 130 | 200 | 178 | 176 | 181 | 139 | 146 | 162 | 163 | 192 | 190 | 141 | 152 |
| 10min | 760 | 218 | 210 | 216 | 193 | 191 | 184 | 229 | 214 | 242 | 242 | 219 | 228 | 246 | 249 | 261 | 266 | 221 | 232 |
| 15min | 793 | 245 | 233 | 237 | 213 | 215 | 220 | 236 | 227 | 261 | 264 | 244 | 258 | 285 | 256 | 281 | 276 | 245 | 245 |
| 20min | 823 | 251 | 238 | 242 | 218 | 221 | 204 | 238 | 232 | 268 | 270 | 259 | 271 | 299 | 300 | 288 | 284 | 256 | 255 |
| 25min | 824 | 257 | 243 | 247 | 223 | 224 | 206 | 240 | 235 | 272 | 272 | 260 | 276 | 305 | 305 | 290 | 282 | 258 | 258 |
| 30min | 822 | 259 | 245 | 249 | 224 | 228 | 207 | 240 | 236 | 273 | 274 | 262 | 279 | 309 | 308 | 291 | 287 | 261 | 260 |
| 35min | 819 | 260 | 247 | 250 | 224 | 227 | 207 | 240 | 237 | 274 | 275 | 265 | 281 | 310 | 310 | 292 | 288 | 262 | 261 |
| 40min | 843 | 260 | 247 | 250 | 224 | 227 | 207 | 241 | 238 | 274 | 274 | 266 | 282 | 311 | 310 | 292 | 288 | 263 | 262 |
| 45min | 847 | 261 | 248 | 250 | 224 | 228 | 207 | 240 | 238 | 274 | 272 | 266 | 281 | 312 | 310 | 292 | 288 | 263 | 262 |

Table 1. The result of stagnation test among multiple commercially available selective coating, notice that we already ruled out Alanod mirosol and mirotherm due to their

performance under a previous test, which testifies the same according to the website information for the supplier. Tinox(Al), Yin(Cu) and Alanod(Sunselect Cu) were considered for pentagon shape XCPC prototyping.

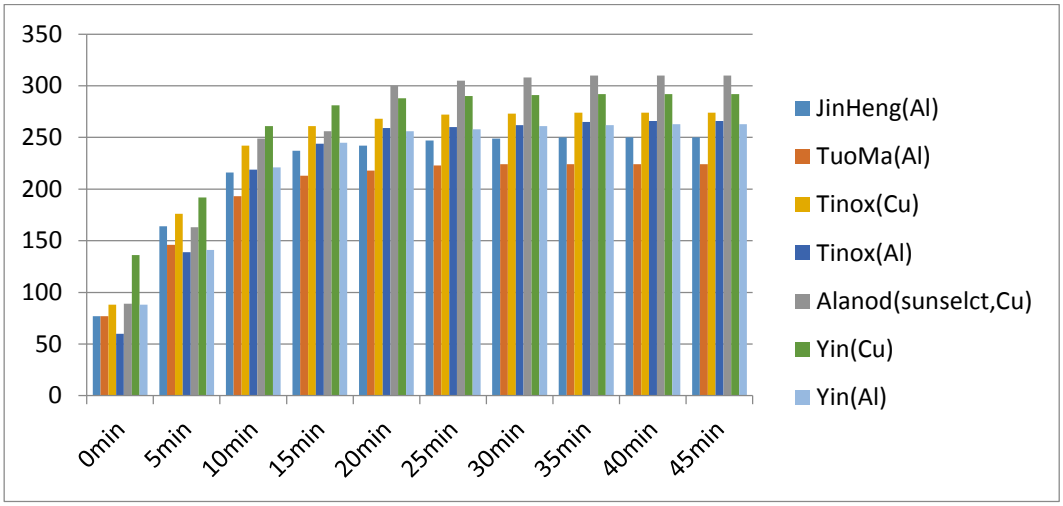


Fig.7 Comparison among multiple commercially available selective coating

Conclusion: Although the stable temperature of a collector at heat balance does not tell directly the emissivity of its selective coating, the result did show an obvious, consistent difference of the performance of various suppliers. During the test we also found that for certain suppliers the coating from different batches of product exhibits huge difference in performance, however, the two German selective coating, Alanod (mirosol, mirotherm and sunselect) and Tinox(Cu, Al) showed stable quality and performance. Based on the choice of the selective coating, we also performed comparison test among the flat absorber and XCPC tubes, refer to the Fig.8

Fig.8 Test between flat absorber evacuated tubes and XCPC.

| Time | Tilted Global | Jinheng (Ch)Pentagon | Jinheng (Ch)102 flat absorber | Alanod(Sunselet Cu)Pentagon | Tinox Cu 102 flat absorber |
|---|---|---|---|---|---|
| 12:28 | 667 | 44 | 59 | 42 | 85 |
| 12:31 | 696 | 102 | 95 | 140 | 134 |
| 12:32 | 686 | 150 | 122 | 219 | 165 |
| 12:34 | 686 | 185 | 153 | 260 | 207 |
| 12:35 | 664 | 206 | 170 | 288 | 228 |
| 12:37 | 678 | 216 | 180 | 302 | 240 |
| 12:38 | 654 | 228 | 191 | 314 | 254 |
| 12:39 | 654 | 232 | 195 | 318 | 258 |
| 12:40 | 653 | 234 | 199 | 320 | 262 |
| 12:41 | 645 | 237 | 202 | 323 | 265 |
| 12:42 | 638 | 240 | 205 | 325 | 270 |
| 12:43 | 634 | 243 | 209 | 326 | 274 |
| 12:44 | 631 | 244 | 211 | 325 | 276 |
| 12:46 | 626 | 244 | 213 | 324 | 278 |
| 12:49 | 635 | 245 | 216 | 324 | 280 |
| 12:51 | 704 | 247 | 219 | 328 | 283 |
| 12:55 | 720 | 252 | 223 | 333 | 289 |
| 12:59 | 726 | 253 | 225 | 332 | 290 |
| 13:01 | 733 | 255 | 226 | 334 | 292 |
| 13:04 | 705 | 255 | 227 | 334 | 293 |
| 13:13 | 693 | 248 | 223 | 327 | 287 |
| 13:23 | 665 | 248 | 226 | 330 | 291 |

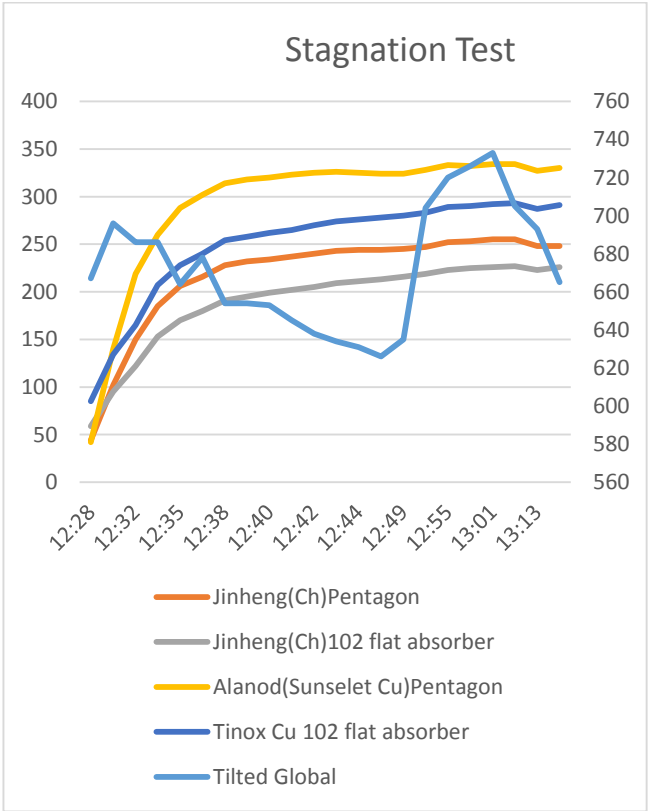

Fig.9 Compared results of various absorbers. The tilted global data is following the secondary y axis on the right.

With even with lower solar condition (665W/m$^2$) (Fig 9), compared to the previous test of 847W/m$^2$,(Fig. 7) the pentagon XCPC sunselect collector still achieved 20°C higher than the flat absorber sunselect, and 40°C more than Tinox flat absorber under the same condition. This showcases the stationary optical concentration of XCPC.

For our collector prototype, we decided to choose the Alanod Sunselect for our next-gen XCPC array.

## 4 Testing and characterization of medium temperature solar collectors.

None of the existing solar testing facilities offer services for medium temperature solar collector with a heat transfer fluid as mineral oil. Therefore we decided to build our own system using the calorimetry method. Multiple iterations of the calorimeter were implemented.

### 4.1 Test stand setup

The advantage of using mineral oil as the heat transfer fluid is its low working pressure. This simplifies the plumbing of a system, but requires a more careful design of the testing stand:

A. No leakage is allowed, because of the fire hazard at a higher temperature.
B. For measurement purposes, calorimeter is needed due to the oil property variation being introduced.
C. Faster fluid speed is required due to less heat transfer capability of oil compared with water.

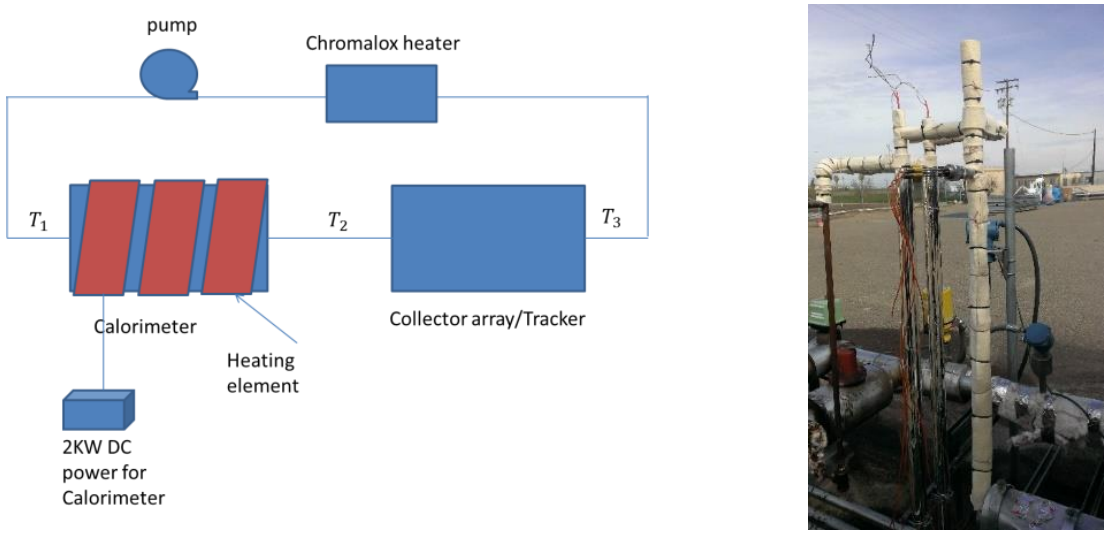


Fig 8. The calorimeter design (a.left) and its insulation process utilizing two vacuum tubes (b.right).

## 4.2 Calorimeter design

Due to the fact that oil properties such as heat capacity and density vary over time with oxidation and impurities, direct measurements of these properties are replaced by electric power measurements using calorimetry. As the same oil steam flows through the calorimeter and the collector array. The mass flow rate and heat capacity of the oil flow will not change

$$Q_{collector} = \dot{m}\, C_p(T_2 - T_3) = \dot{m}\, C_p \Delta T_{collector} \tag{11}$$

$$Q_{calorimeter} = \dot{m}\, C_p(T_1 - T_2) = \dot{m}\, C_p \Delta T_{calorimeter} \tag{12}$$

From equation (9) and (10), we can get $Q_{collector} = \frac{\Delta T_{collector}}{\Delta T_{calorimeter}} \cdot V_{cal} \cdot I_{cal}$ (13)

Where $\Delta T_{calorimeter}$ is the temperature rise across the calorimeter, measured by thermocouple clusters, $V_{cal} \cdot I_{cal}$ gives the power of the calorimeter heating up the mineral oil. The calorimeter is well insulated to control the heat loss and other errors to be below 2% of the calorimeter input. (Fig.(b))

To insulate the calorimeter's two heating elements well, we used evacuated tubes, with additional insulation inside to eliminate the effect of environment temperature changes. To compare the result with a standard method using flow rate measurements, we implemented a Coriolis flow meter to compare with the results from equation (11).

4.3 Calibration of the calorimeter

Based on the principle stated above, we performed numerous tests to make sure the calorimeter can function as expected under stabilized state. Fig.2 shows the process of calibrating and compensating for the heat loss. In such a process, we maintain the flow rate of the loop at a constant level of 100±10gram/second, and observe the effect of modulating the power input of the calorimeter, namely, the change of the temperature difference between the inlet and outlet of the calorimeter. The flow rate is closely monitored by a precise Coriolis flow meter (mass flow rate error of 0.02%). In Fig.8 the x-axis is the flow rate multiplied by the temperature, y-axis is the power input of the calorimeter calculated by the product of voltage and current input, which are measured up to the accuracy of 0.1%. If we ignore the small heat capacity change caused the temperature change between the inlet and outlet (about ±2% of total oil heat capacity), the result should be a linear curve, with the tangent being the heat capacity of the working fluid. This turns out to be true, with a linear fitting RMS of 0.0135 for a linear fitting of 7 points as shown in Fig. 9. The plot also provides an estimation of the heat loss under every temperature we tested the collector for, which is typically under 100 Watts, such an estimate of the heat loss cannot be accurate because it includes the error produced by any of the remaining error from the calibration of the thermocouples. In our characterization process, we use the Y-intersect from the linear fitting as a combination of heat loss and thermocouple error. In the end we compensated for this

error in the calculation for each efficiency measurement according to the testing temperature. Each data point on Fig. 10 corresponds to a data set of Fig.9.

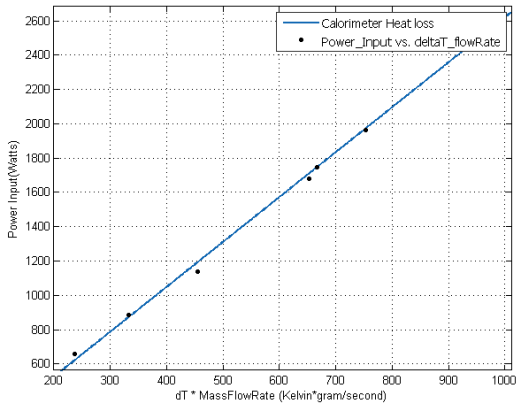


Fig.9. The heat loss linear fit according to the power input and $\dot{m}\,\Delta T$, measured at 150 °C. The RMS error is 36.9 watts, or 1.35% error according to the regular input of 2KW. R-Square is 0.9975 for the linear fitting.

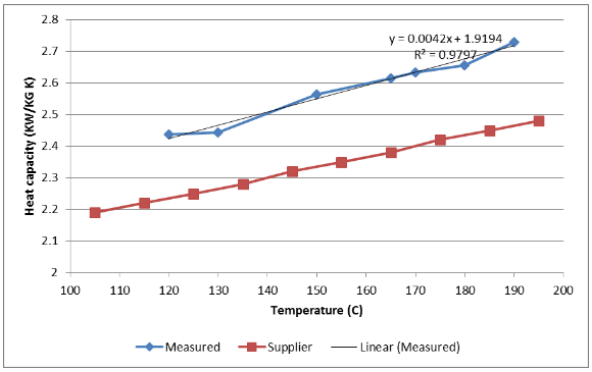


Fig.10. The measurement of heat capacity to provide a comparison with the datasheet from the supplier of the mineral oil.

The calibration process also gives us the heat capacity of the mineral oil that we are using. However we do not need to have this information for correctly measuring the characteristic curve of the collector. It is remarkable that the mineral oil, due to oxidation, is about 10% to 20% above the heat capacity number provided by the data from the supplier (Fig.10). It is also changing according to a temperature in a roughly linear fashion. In the commonly used flow rate method, where the heat capacity (such as water) is estimated or sampled by the characterization lab, the result relies on the accurate measurement of both the flow rate and heat capacity. The uncertainty in the heat capacity in this case shows how inaccurate it would be if we chose to use the data provided by the supplier. A commonly practiced flow rate method will mislead us to believe in a much lower efficiency of the collector. Fig.11 shows the stability of the testing loop. The sampling rate is 2 second per point. After the power was turned off at

point 980, the $\Delta T_{Cal}$ (grey line) showed a delayed response (about 15 second) and then an exponential drop approaching zero. However, because of the heat loss of the calorimeter and the calibration error of the thermocouple clusters, it stabilizes at about -0.9 °C. The time required to reach such a stable state is 3.7 minutes. Therefore in our characterization process we allowed a stable interval of 10 minutes between the sampling of each data, if the calorimeter power has been changed.

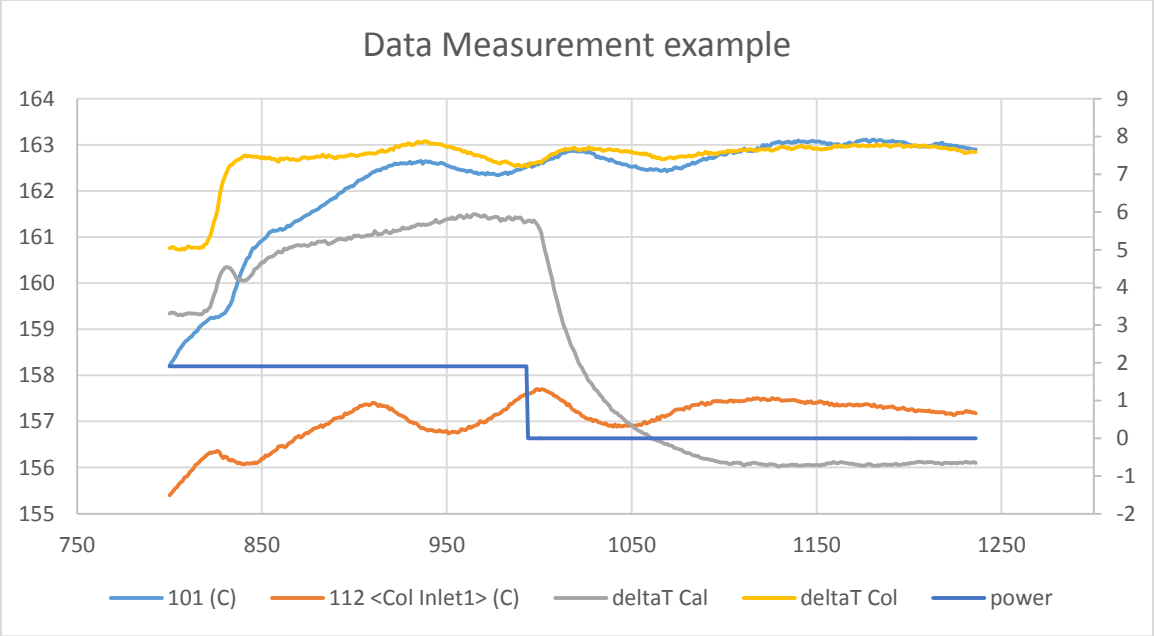


Fig.11. The calorimeter inlet temperature, one of the five on the inlet cluster(101), The collector inlet temperature(112), one of the 3 on the cluster, the reading of these two follow the left y axis and read around temperature 160°C. The $\Delta T_{cal}$, $\Delta T_{col}$, the power calculated from$V_{cal} \cdot I_{cal}$ (in Kilowatts). These numbers follow the right y axis and the reading is between -2 to 9. Flow rate is stable at 155grams/second.

## 5 Testing with two novel mid-temperature solar collectors

### 5.1 The testing of novel pentagon shape absorber XCPC

In the design for eXternal Compound Parabolic Concentrator (XCPC), the absorber tube is preferably a metal glass vacuum tube due to its improved heat transfer capability compared to the all glass vacuum tubes.[6] We have since prototyped East-West XCPC

using pentagon absorber as cross section.(Fig.13) The testing condition and the results are shown in the Table 2. In our testing the collector is faced directly normal to the sun direction. Although the IAM is not measured, our optical ray tracing program provides us with a good understanding of how the efficiency of the collector changes according to the incident angle of the sunshine. (Fig.12.a) The optical efficiency in this figure is calculated according to the angle in the transversal plane (Fig.12.b). In a standard testing this will have to be multiplied with the cosine effect of the collector plane to produce the IAM. The 5-8% loss at various angle is produced by the gap between the absorber and the tip of the reflector. This loss is unavoidable with the ideal concentrator design, but can be reduced by lowering the concentration ratio using a V or W groove [14][15]. In our design, the gap has been controlled to be only 3mm out of the 272 mm circumference of the pentagon shape. We considered it unnecessary to make this trade off with additional design complexity of the concentrator. The result is showing that such a small gap loss is not affecting the general performance of our collector.

Table.2 shows the result of the test under various temperature. The efficiency based on the flow rate method is closely related to the result based on the calorimetry. The averaged difference is 2.2%. The thermocouple has an accuracy of ±0.1°C. The inlet outlet temperature difference of the collector is controlled within 8°C. Therefore the results of the two different testing method is at the level of the thermocouple error. Fig.14 shows how the trend of the results of the two testing method are closely matched.

| Testing temperature(Celsius) | 160 | 200 | 230 |
|---|---|---|---|
| Calorimeter $T_{out}$-$T_{in}$ (Celsius) | 6.08 | 4.89 | 4.07 |

| | | | |
|---|---|---|---|
| Collector $T_{out}$-$T_{in}$(Celsius) | 7.48 | 6.24 | 4.99 |
| Calorimeter T average(Celsius) | 170.7 | 204.49 | 231.29 |
| Collector T average(Celsius) | 165.22 | 200.72 | 229 |
| Incidence Irradiance(Based on 4.5 $m^2$ aperture area)(KW) | 4.19 | 4.19 | 4.11 |
| Collector power based on Calorimetry(KW) | 2.33 | 2.23 | 1.84 |
| Efficiency based on Calorimetry | 55.67% | 53.37% | 44.80% |
| Collector power based on flow rate method(KW) | 2.44 | 2.15 | 1.76 |
| Efficiency based on flow rate method | 58.31% | 51.36% | 42.78% |
| Oil heat capacity calculated (KJ/Kg.Celsius) | 2.9 | 3.04 | 3.16 |
| Flow rate(grams/second) | 112.45 | 113.11 | 111.61 |
| Tilted Global Irradiation($W/m^2$) | 930.54 | 930.15 | 913.84 |
| Direct Normal Irradiation($W/m^2$) | 838.89 | 855 | 829.33 |

Table 2. The testing results of XCPC with pentagon shape absorber.

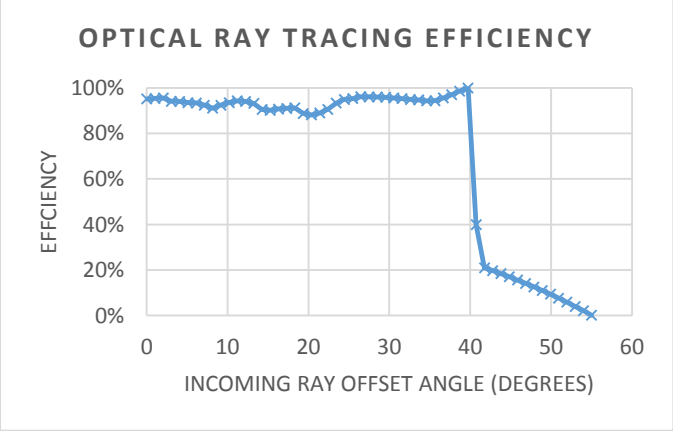


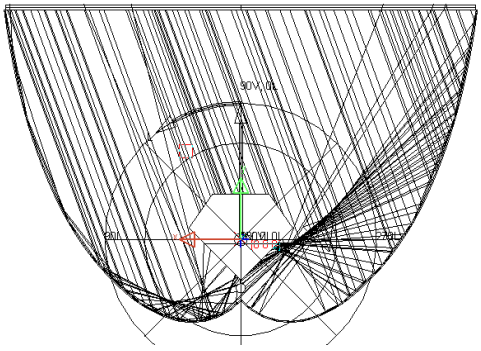

Fig.12 (a) The ray tracing result showing the optical efficiency of an E-W XCPC setup. Notice the effects 5-8% optical loss due to (b) gap loss and bottom heat transfer channel for the absorber.

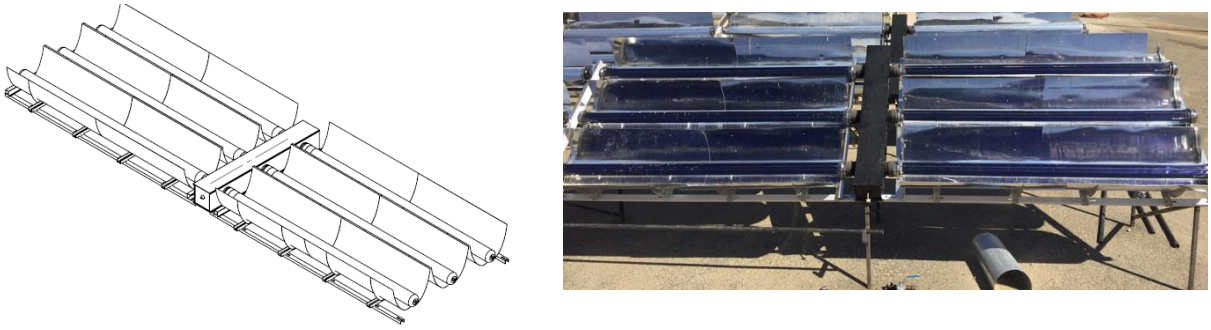

Fig.13 . The XCPC collector with east west axis direction, sharing manifold in between. Aperture area for each collector is 4.5 $m^2$

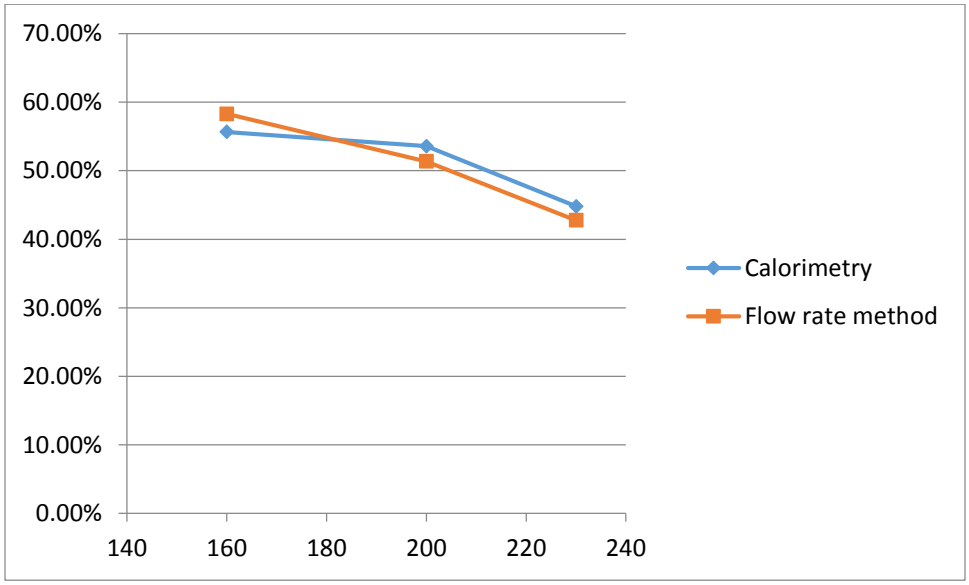


Fig.14. The efficiency measured with Calorimetry and the flow rate method.

5.2 The small demonstration project of pentagon shape absorber XCPC

A demonstration array of 16 pentagon shape absorber XCPC is setup for a boiler preheating project. Due to the constraint of the floor planning, instead of facing directly

EW, the axis of the collectors were 20 degrees off. This resulted in a late start between 10:00 and 10:30 in the morning. (Fig.15)

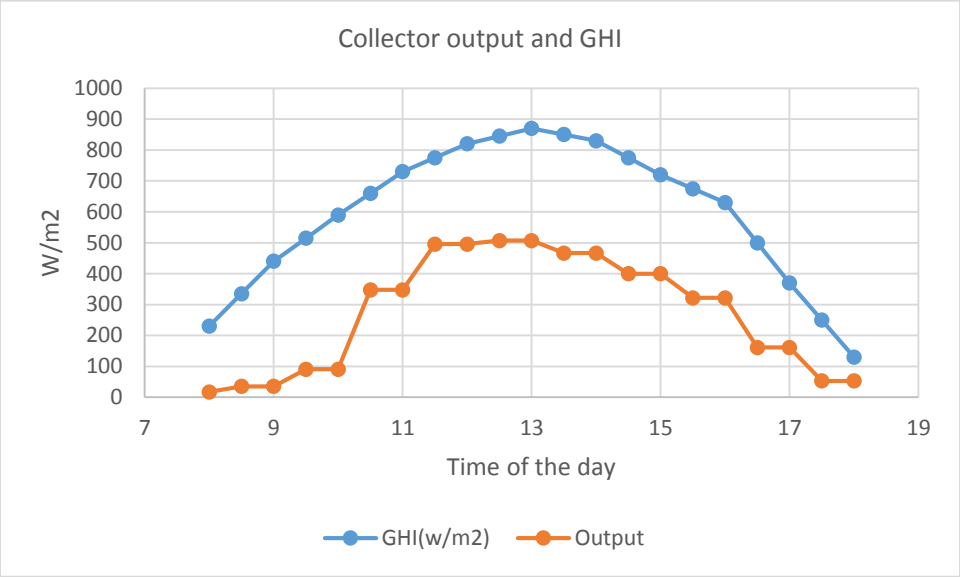


Fig 15. A typical day result for the XCPC array.

| Time | Ambient | Flow rate | Inlet | Outlet | Delta T | Energy harvested | | Output | |
|---|---|---|---|---|---|---|---|---|---|
| | deg C | Lt/hr | deg C | | | kcal | kWh | kW | Watts/m2 |
| | | | | | | | | | |
| 7 | 37 | 535 | 40 | 41 | 1 | 267.5 | 0.315 | 0.629 | 17.484 |
| 7.5 | 38 | 533 | 40 | 41 | 1 | 266.5 | 0.314 | 0.627 | 17.418 |
| 8 | 38 | 533 | 40 | 41 | 1 | 266.5 | 0.314 | 0.627 | 17.418 |
| 8.5 | 38 | 544 | 41 | 43 | 2 | 544 | 0.640 | 1.280 | 35.556 |
| 9 | 38 | 544 | 41 | 43 | 2 | 544 | 0.640 | 1.280 | 35.556 |
| 9.5 | 40 | 556 | 42 | 47 | 5 | 1390 | 1.635 | 3.271 | 90.850 |
| 10 | 40 | 556 | 42 | 47 | 5 | 1390 | 1.635 | 3.271 | 90.850 |
| 10.5 | 40 | 560 | 43 | 62 | 19 | 5320 | 6.259 | 12.518 | 347.712 |
| 11 | 40 | 560 | 43 | 62 | 19 | 5320 | 6.259 | 12.518 | 347.712 |
| 11.5 | 40 | 562 | 43 | 70 | 27 | 7587 | 8.926 | 17.852 | 495.882 |
| 12 | 40 | 562 | 43 | 70 | 27 | 7587 | 8.926 | 17.852 | 495.882 |
| 12.5 | 40 | 554 | 43 | 71 | 28 | 7756 | 9.125 | 18.249 | 506.928 |
| 13 | 40 | 554 | 43 | 71 | 28 | 7756 | 9.125 | 18.249 | 506.928 |
| 13.5 | 38 | 549 | 42 | 68 | 26 | 7137 | 8.396 | 16.793 | 466.471 |
| 14 | 38 | 549 | 42 | 68 | 26 | 7137 | 8.396 | 16.793 | 466.471 |
| 14.5 | 38 | 556 | 42 | 64 | 22 | 6116 | 7.195 | 14.391 | 399.739 |
| 15 | 38 | 556 | 42 | 64 | 22 | 6116 | 7.195 | 14.391 | 399.739 |
| 15.5 | 37 | 547 | 41 | 59 | 18 | 4923 | 5.792 | 11.584 | 321.765 |
| 16 | 37 | 547 | 41 | 59 | 18 | 4923 | 5.792 | 11.584 | 321.765 |
| 16.5 | 34 | 549 | 41 | 50 | 9 | 2470.5 | 2.906 | 5.813 | 161.471 |
| 17 | 34 | 549 | 41 | 50 | 9 | 2470.5 | 2.906 | 5.813 | 161.471 |
| 17.5 | 32 | 541 | 40 | 43 | 3 | 811.5 | 0.955 | 1.909 | 53.039 |
| 18 | 32 | 541 | 40 | 43 | 3 | 811.5 | 0.955 | 1.909 | 53.039 |
| 18.5 | 30 | 534 | 39 | 38 | 0 | 0 | 0 | 0 | 0 |
| 19 | 30 | 534 | 39 | 38 | 0 | 0 | 0 | 0 | 0 |
| | | | | | | kcal | kWh | kWh/m2 | |
| Total Energy recovered per day | | | | | | 88910.5 | 104.601 | 2.906 | |

Table 3. Detailed information of a typical day for the demonstration array.

# 6 Design and testing of the ICPC collector

## 6.1 The first iteration of the ICPC design

The first stage of the design was to decide about the assembly of different parts of the ICPC. The technology employed to assemble the receiver

A. Receiver structure

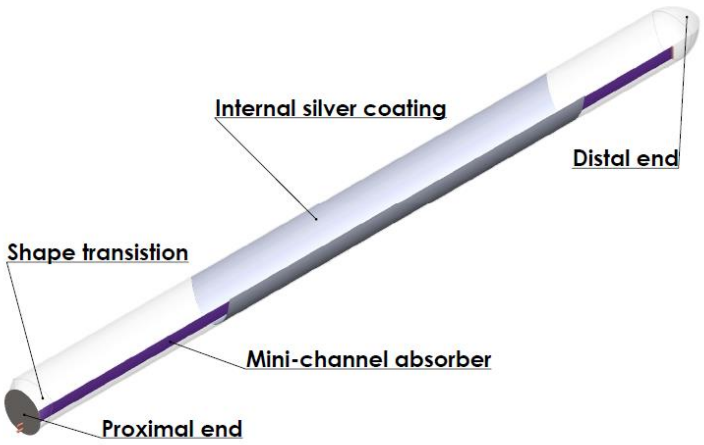


Figure 16 Structure of the Itegrated Receiver

Figure 16 shows the receiver structure. The proximal end consists of the metal glass seal and absorber transition. It also includes a transition of the glass tube from the concentrator shape to cylindrical shape. The middle part of the receiver consists of the absorber with a selective coating, and an internal silver coating on the glass tube inner surface, which is shaped according to the optics design. The distal end consists of the closing up of the glass tube and the freely expanding end of the absorber. (The gas getter and supporter of the absorber is omitted in this graph.)

B. The optics

It is crucial to maintain the current IO design within a small cost increment compared to the original design. The recent improvement of technology in metal glass compression sealing and borosilicate 3.3 glass tube manufacturing has offered us an unprecedented opportunity to demonstrate such a tube at low cost. Additionally we are going to show that a single end sealing will help to reduce the cost even more by omitting bellows and the assemblies needed to mitigate thermal expansion in existing vacuum tube technologies.

First, it should be emphasized that the receiver shape can be any convex shape for the IO. The two geometries shown in Figure 17 and Figure 18 shows practical double sided absorber architecture consistent with glass tube shaping technologies.

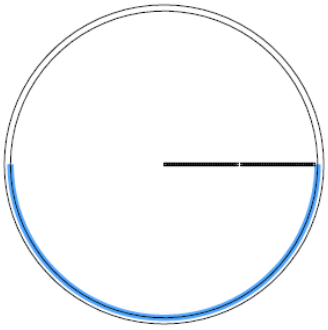

Figure 17 Asymmetric tubular design

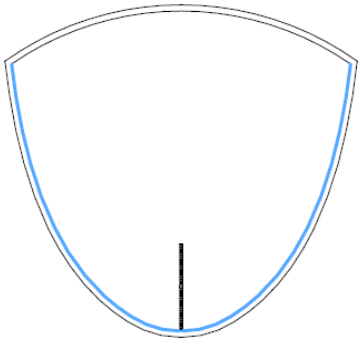

Figure 18 Nonimaging design

Figure 17 shows the asymmetric concentration using a 102mm diameter cylindrical tube. Figure 8 shows the nonimaging design using the same diameter tube, but re-shaped in situ using a nonimaging optics design to achieve a 1.93 concentration ratio at 30 degrees acceptance angle. The bottoms of both tubes are coated with silver at 97% reflectance. Both tubes are using flat absorbers as the optic target. The asymmetric design is at concentration ratio of 1:1; however, because it is using both sides of the absorber, its heat loss area will be half of a simple plate absorber receiving light on just one side. The nonimaging optics design is additionally multiplying the double side effect with its concentration ratio. Figure 9 shows the ray tracing of the wide angle nonimaging concentrator design.

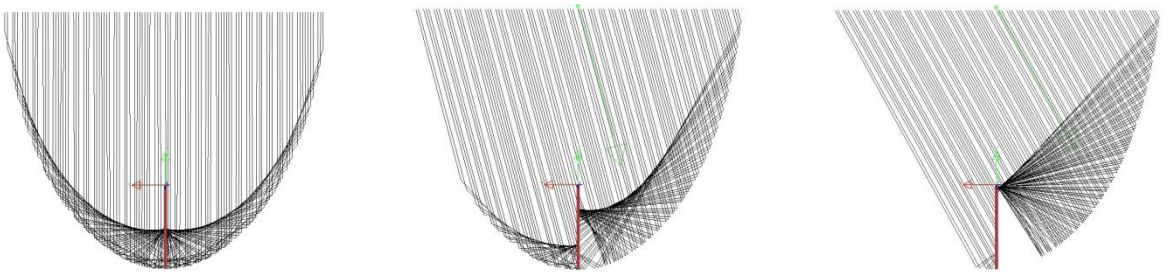

Figure 19 Ray tracing for the ICPC with a double sided absorber

c)The proximal end

There are two candidate technologies for the metal glass seal. The first candidate is the housekeeper seal (Figure 20) which has existed for the last 40 years. The housekeeper seal can be done on a small diameter (5mm to 60mm) on a glass lathe with the sealing point heated to above 1000˚C. The matching kovar is a standardized product and can be readily purchased. The second candidate is the more recently developed thermal compression seal (Figure 20). Unlike the housekeeper seal it requires a lower sealing temperature (300˚C using lead and 600˚C using aluminum). This seal is cheaper compared to housekeeper seal when it comes to mass production. In both scenarios the metal glass seal is at a much lower temperature compared to the working fluid temperature due to the temperature gradient on the kovar. This gradient can also be engineered with the consideration of thermal stress in mind to keep the seal point at a temperature below 300˚C (as shown on the right).

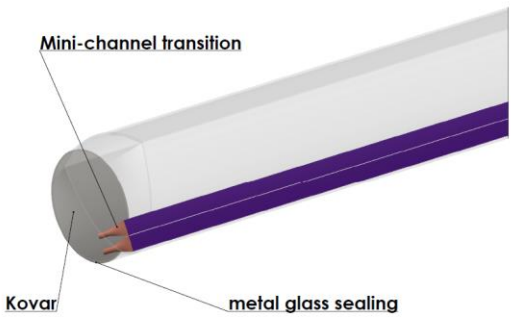


Figure 20 Proximal End

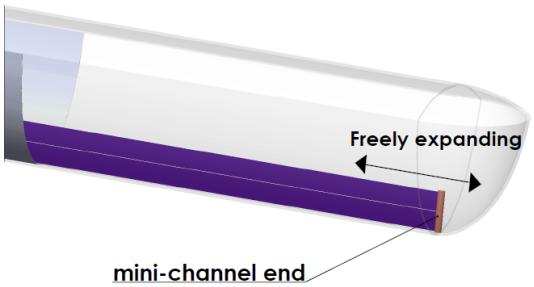


Figure 21 Distal End

d)The distal end

The free expansion of the absorber on the distal end allows the absorber to slide on its long axis at its working temperature without putting any pressure on the metal glass seal or the glass tube. This design omits the bellows used in the standard seal shown in Figure 9. The force exerted on the slim absorber by the double end sealing is also removed with a single end seal, reducing the risk of deformation under higher working temperature. The end of the absorber is then induction welded with the same high temperature enduring silver alloy.

Figure 22 From left to right: housekeeper seal, thermal compression seal (the silver color inside of the tube is the barium getter), and the double end seal using bellows for the UVAC series tubes.

e) The tube body

The absorber is coated with selective coating at 95% absorptivity and < 10% emissivity. The material in this case can be chosen from W/Al2O3, Mo/ Al2O3, and Ti/AlNx. The sputtering machine for 2.5 meters absorbers can be easily found with modest time charge in vacuum tube production facilities. The sputtering target can be purchased and then applied to the existing target.

The shaping of the glass tube according to the IO design can be achieved using a graphite mode pressing on the glass tube as it is pulled from the electric glass oven. The borosilicate 3.3 tube production facility that we have contact with is already experimenting on the accuracy of such a process. They are already using this process to produce lighting decorations at this moment. It will be an in-situ process without additional material cost or the second time heating cost except for the first time cost of building the graphite mode.

The reflective layer can be deposited using the chemical silver deposition process or the metallic evaporation of aluminum. The prior has a proven reflectivity of 97% and the latter 87-92%. Because this reflective layer will be under the protection of vacuum, there is no risk of environmentally caused degradation.

6.2 The second iteration and the stress analysis

During our second stage of prototyping, the vacuum tube imploded after the baking of the vacuum was finished. A preliminary check with a polarity surface tension machine found that the tension of the glass is around 15MPa. This number is under the quality control of a glass tube. However, glass with a noncircular cross section under the pressure of one atmosphere is approaching the glass tension limit of 30MPa. A tension analysis was performed within solidworks finite element analysis.

The thickness of the glass tube had to be increased, with the glass tube top window shaped as a dome.( This improvement reduced the maximum tension induced by the vacuum to be below 9MPa. Leaving enough room for the remaining glass tension after the annealing.

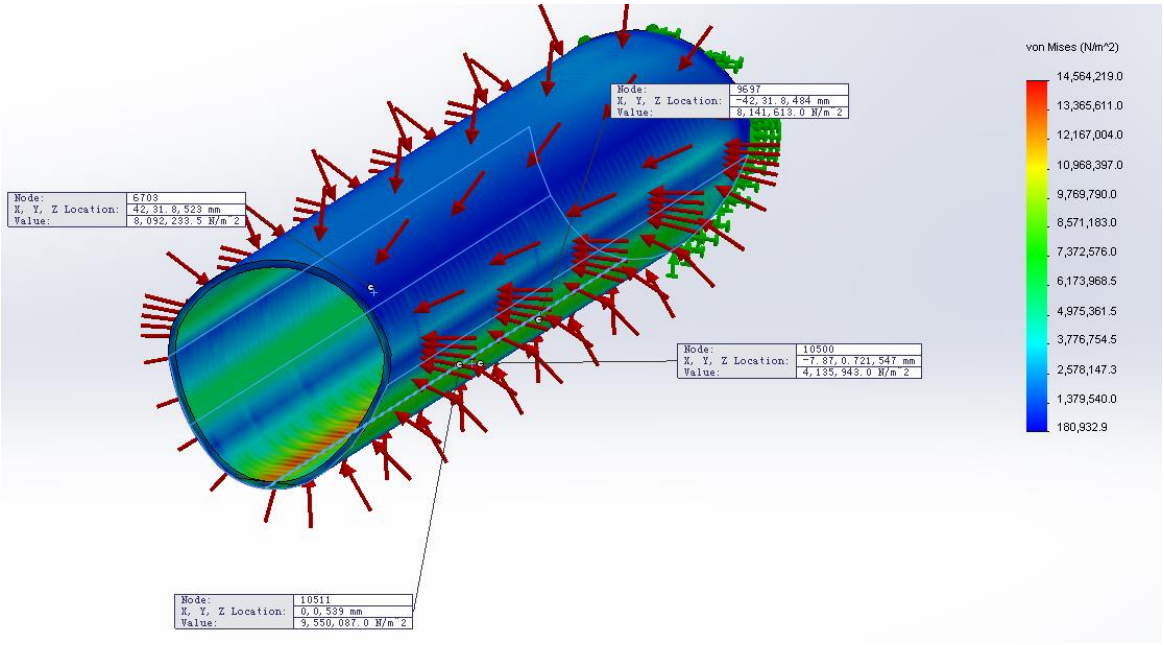


Figure 23 The final shape for the ICPC glass tube based on the tolerance of additional glass tension induced by on atmosphere pressure.

Through the adjustment of the glass tube. A half meter prototype is produced. It included a functioning heat pipe. Fin tube structure was implemented for the ease of welding the fluid channel through the stainless kovar.(Fig.25)

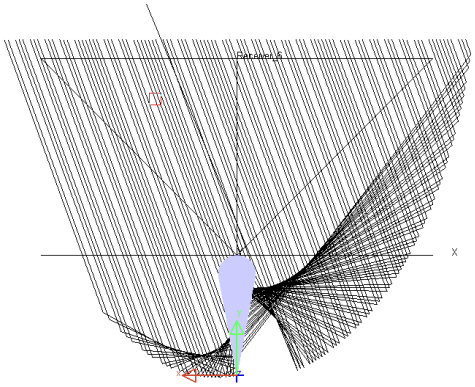

Fig.25 The ICPC half meter prototype, on the right, the icecream cone cross section of the absorber for the ease of fabrication.

## 6.3 The ICPC prototype array

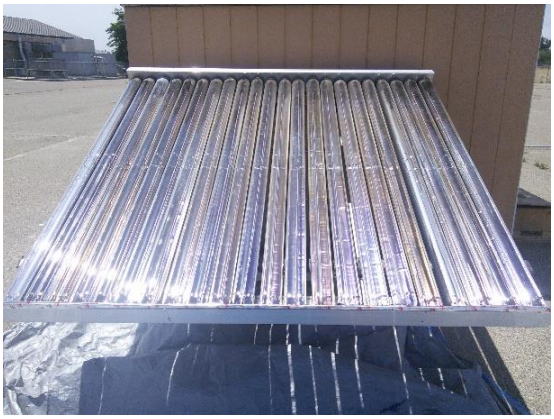

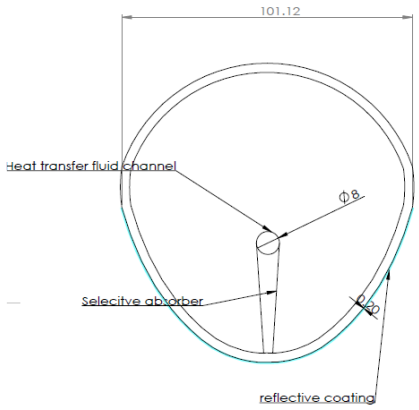


Fig.25. a) The ICPC 3.5m2 prototype, with full 1900mm length tube, front view.

b) The cross section of the original ICPC prototype design. The CPC shaped collector is integrated into the shape of the glass tube. The absorber is perpendicularly positioned in the evacuated tube.

In the third stage of the prototype. The full size collector of ICPC is fabricated and tested (Fig.25). Each of the ICPC tube is eventually fabricated at 85mm width with an absorber of 30mm height, resulting in a concentration ratio of 1.41. The aperture area is 1900mm X 85mm for each tube. A heat pipe of 8mm diameter is inserted into the absorber fin and ultrasonic welded on to the fin to ensure the heat transfer. The reflective coating is using the standard silver mirroring chemical process, with a

protective resin to be weather proof. The gap loss between the absorber and the reflector is averaged between 2.5mm to 3mm. The full array efficiency is shown in Fig.25. The IR imaging for the thermal loss is shown in Fig.8. The optics of the ICPC is designed for a 35 degrees acceptance angle and therefore should be positioned east-west direction. But for testing purpose and the trial of the heat pipe as a heat transfer model, we implemented them as north-south aligned, and put them on a tracker to take the measurement. The result is showing a relatively lower performance compared to the XCPC model under the same temperature. However, this is mainly due to the heat pipe not functioning as ideally as a heat transfer mechanism compared to the direct flow mechanism in the XCPC array.

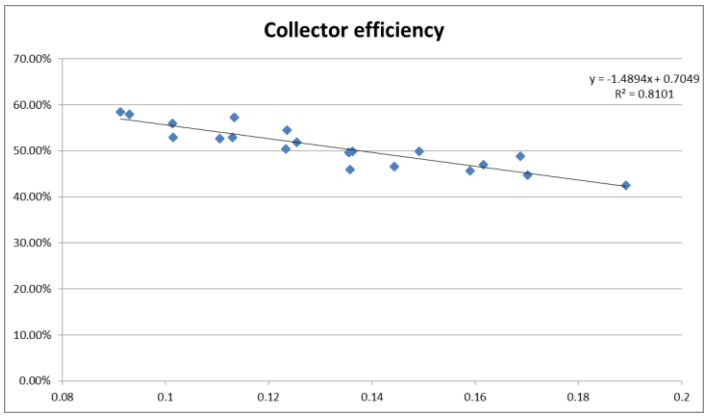


Fig.26 The collector efficiency according to $T^*=(T_m-T_a)/I$

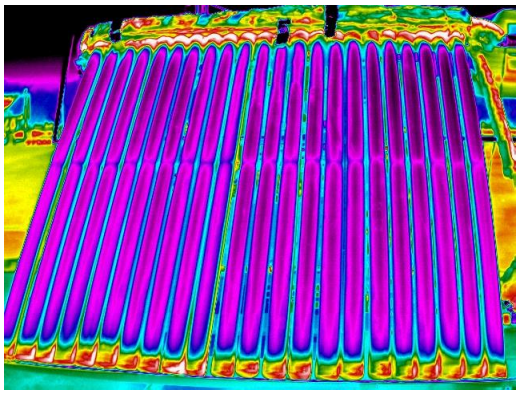

Fig.27. The result of the thermal imaging showing the heat loss.

## 7 Discussion

In this thesis, two novel, medium temperature solar thermal collectors with oil as the heat transfer fluid are presented. These prototypes are at different stage for demonstration. Both of them benefitted from new optics which allowed the absorber shape to be customized according to the ease of production. The findings of a 4.5 m2

XCPC array and a 3.5 m2prototype ICPC array are presented. The calorimeter testing method has its advantage of solving the issue of constant fluctuation of the heat capacity of mineral oil over time. This issue is resolved by replacing the hard to measure parameters such as flow rate and heat capacity with easy to measure parameters such as voltage, current, and temperature. The data has shown that this method is stable and reliable for understanding the collector efficiency despite a constantly changing outdoor environment and degradation of the working fluid. The XCPC and ICPC collectors showed 52% and 42% efficiency, respectively, at 200 °C based on global irradiance.

## References


[1] "IEA SHC world wide 2013," 2013. [Online]. Available: http://www.iea-shc.org/data/sites/1/publications/Solar-Heat-Worldwide-2013.pdf.

[2] R. Winston, "Thermodynamically efficient solar concentrators," *J. Photonics Energy*, vol. 2, no. 1, p. 025501, Apr. 2012.

[3] S. Fischer, W. Heidemann, H. Müller-Steinhagen, B. Perers, P. Bergquist, and B. Hellström, "Collector test method under quasi-dynamic conditions according to the European Standard EN 12975-2," *Sol. Energy*, vol. 76, no. 1–3, pp. 117–123, Jan. 2004.

[4] "ISO 9806:2013." [Online]. Available: http://www.iso.org/iso/catalogue_detail.htm?csnumber=59879.

[5] "SPF Collector Testing Explanation." [Online]. Available: http://www.solarenergy.ch/index.php?id=203.

[6] L. Ma, Z. Lu, J. Zhang, and R. Liang, "Thermal performance analysis of the glass evacuated tube solar collector with U-tube," *Build. Environ.*, vol. 45, pp. 1959–1967, 2010.

[7] J. J. O'Gallagher, "Nonimaging Optics in Solar Energy," *Synthesis Lectures on Energy and the Environment: Technology, Science, and Society*, vol. 2. pp. 1–120, 2008.

[8] R. Winston, J. C. Miñano, and P. Benítez, *Nonimaging Optics*. Academic Press, 2005, p. 497.

[9] A. Rabl, *Active Solar Collectors and Their Applications*. Oxford University Press, USA, 1985, p. 517.

[10] M. F. Modest, *Radiative Heat Transfer*. Academic Press, 2013, p. 904.

[11] R. Winston and W. Welford, "Geometrical vector flux and some new nonimaging concentrators," *J. Opt. Soc. Am*, 1979.

[12] "Example of SPF Test Report." [Online]. Available: http://www.solarenergy.ch/fileadmin/daten/reportInterface/kollektoren/factsheets/scf1391en.pdf.

[13] "Alanod Absorption Product Info." [Online]. Available: http://www.bluetec.eu/en/Absorption/Products.

[14] W. McIntire and R. Winston, "Design considerations for reducing optical losses due to gaps between absorbers and their reflectors," *Proc. Annu. Meet.-Am. Sect. Int. Sol. Energy Soc.;( …*, 1981.

[15] W. R. McIntire, "New reflector design which avoids losses through gaps between tubular absorbers and reflectors," *Sol. Energy*, vol. 25, no. 3, pp. 215–220, Jan. 1980.

# Appendix A

## ReverseAnyCPC.m

```
% reverse the CPC forming process and direct the light from the absorber.
clear;
clf;
delete('CPC.xls','Absorber.xls','sampledData.xls');
global g_unitLength;
g_unitLength = 6;

%% minimal step for the shape, the smaller the more accurate.
global g_minStep;
g_minStep = g_unitLength/1000;

prompt = 'What is the accuracy you want? (0-100) per cent';
def = {'40'};
dlg_title = 'Input';
num_lines = 1;
accuracy = inputdlg(prompt,dlg_title,num_lines,def);
accuracy = str2double(accuracy(1));
best = 0.00001;%100
worst = 0.7;%0
% expression:a*log(x)+b = accuracy;
a = 100/(log(best)-log(worst));
b = 100-a*log(best);
global g_minStepRatio;
g_minStepRatio = exp((accuracy-b)/a);
global g_absoberShapes;
g_absoberShapes =
{'Pentagon','MiniChannel','SimpleCircle','CircleWithGapConsideration','58mm
absorber icecream cone design','85mm absorber icecream cone design','hand
drawn 1','hand drawn 2','Octagon','random points','changed
shape','square','flat','improvedPentagon', 'oval shape','v groove'};
global g_absorber;
g_absorber = [];
prompt = 'What is the half acceptance angle? (0-90) degrees';
def = {'45'};
dlg_title = 'Input';
num_lines = 1;
hAcceptance = inputdlg(prompt,dlg_title,num_lines,def);
hAcceptance = str2double(hAcceptance);
% hAcceptance
global g_acceptanceAngle;%change the number in degree
g_acceptanceAngle = hAcceptance/180*pi;
global g_barPos;%% bar position according to its crossing on X axis in ratio
to the apperature
g_barPos=(1/2)*cot(g_acceptanceAngle);
global g_shapeData;
g_shapeData = [];
%% truncating according to the point counts,>0 <1
prompt = 'What is the truncation ratio according to ideal aperture? (0-100)
per cent';
def = {'95'};
dlg_title = 'Input';
```

```
num_lines = 1;
trancation = inputdlg(prompt,dlg_title,num_lines,def);
trancation = str2double(trancation);

global g_truncatingPercentage;
g_truncatingPercentage=trancation/100;

% shapeName = questdlg('Choose absorber',...
%     'What is the absorber shape?,Excel files should be closed!',...
%     'MiniChannel','Pentagon','Pentagon');
% %'Circle','SimpleCircle','CircleWithGapConsideration'
[shapeNumber,v]=listdlg('PromptString','What is the shape?',...
    'SelectionMode','single',...
    'ListString',g_absoberShapes);
if(v==1)
    Absorber(shapeNumber);
else
    return;
end;
figure(1);
plot(g_absorber(1,:),g_absorber(2,:));
axis equal;
hold on;
absorberExcelData = [];
for i = 1:size(g_absorber,2);
    pointStr = {sprintf('%.2fmm',g_absorber(1,i)),
sprintf('%.2fmm',g_absorber(2,i)),'0mm'};
    absorberExcelData = [absorberExcelData;pointStr];
end;
%% calc the absorber area(length)
absLength = 0;
for i = 2:size(g_absorber,2);
    absLength = absLength+norm(g_absorber(:,i)-g_absorber(:,i-1));
end;

idealApertureLength = absLength/sin(g_acceptanceAngle);


i=1;
A = g_absorber(:,i);
B = g_absorber(:,i+1);
%C = g_absorber(:,i+2);
P = A;
g_shapeData = P;
%% stage = 0:involute;1:reflecting to particular angle;2:finish
stage = 0;
%wordCount = 1;
xlsData = [];
arcLength = 0;

while(stage < 2)
    A = g_absorber(:,i);
    B = g_absorber(:,i+1);
    % to avoid the case that the absorber is not closed, keep the C as it
    % is.
%     if(i+2<=size(g_absorber,2))
```

```
%         C = g_absorber(:,i+2);
%     end
    currP = P;
    %% this only needs to be checked when the stage is still 0, i.e. barPoint
needs to be checked for the current
    %% P so that the program knows when to change to the second stange
    %% the sliding bar position:y=tan(g_acceptanceAngle)x+g_barOffset
    % bar perpendicular crossing point position
    if(stage == 0)
        tang=tan(g_acceptanceAngle);
        x_bar = (P(1)+tang*P(2)-
tang*idealApertureLength*g_barPos)/(tang^2+1);
        y_bar = tang*x_bar+idealApertureLength*g_barPos;
        barPoint = [x_bar;y_bar];
    end;
    %writePos = sprintf('A%d',wordCount);
    pointStr = {sprintf('%.2fmm',P(1)), sprintf('%.2fmm',P(2)),'0mm'};
    xlsData = [xlsData;pointStr];
    %wordCount= wordCount+1;
    PB = B-P;
    PBar = barPoint-P;
    if(CrossProduct(PB,PBar)>=0)
        stage = 0;
    elseif(P(1)>1/2*idealApertureLength*g_truncatingPercentage && P(2)>=B(2))
        stage = 2;
    else
        stage = 1;
    end
    %currPoint = g_absorber(:,1);
    if(stage==0)
        %pause(0.02);
        %old
%             newY = currP(2)-(B(1)-currP(1))*g_minStepRatio;
%             newX = currP(1)+(B(2)-currP(2))*g_minStepRatio;
%             P = [newX;newY];
%           new method, N is the mid point
        N = [0 0];
        N(2) = (currP(1)-
B(1)+g_minStepRatio*B(2)+1/g_minStepRatio*currP(2))/(1/g_minStepRatio+g_minSt
epRatio);
        N(1) = g_minStepRatio*(B(2)-N(2))+currP(1);
        P(1) = 2*N(1)-currP(1);
        P(2) = 2*N(2)-currP(2);
        plotLine(P,B);
    elseif(stage==1)
        %using flow line, the direction should be (g_acceptanceAngle+pi/2)
        %+ angle of BP divided by 2
        sinBP = (P(2)-B(2))/norm(PB);
        cosBP = (P(1)-B(1))/norm(PB);
        tanDir =
(sin(g_acceptanceAngle+pi/2)+sinBP)/(cos(g_acceptanceAngle+pi/2)+cosBP);
        cosDir = sqrt(1/(1+tanDir^2));
        sinDir = tanDir/sqrt(1+tanDir^2);
        newX = cosDir*norm(B-P)*g_minStepRatio+ currP(1);
        newY = sinDir*norm(B-P)*g_minStepRatio+ currP(2);
        P = [newX;newY];
```

```
        %% the sliding bar
position:y=tan(g_acceptanceAngle)x+idealApertureLength*2
        % bar perpendicular crossing point position
        tang=tan(g_acceptanceAngle);
        x_bar = (P(1)+tang*P(2)-
tang*idealApertureLength*g_barPos)/(tang^2+1);
        y_bar = tang*x_bar+idealApertureLength*g_barPos;
        barPoint = [x_bar;y_bar];
        % the current barPoint is associated with the last P, need to plot
        % it first.
        plotLine(P,barPoint);
        plotLine(P,B);

    else
        break;
    end;
    plotLine(currP,P);
    plotLine([-currP(1),currP(2)],[-P(1),P(2)]);
    arcLength = arcLength+norm(currP-P);
    g_shapeData = [g_shapeData,P];
    %% find next point
    %PA = A-P;
    if( i+2 <= size(g_absorber,2)) % the finding of the tangent line has to
meet the condition of not running out of points, especially the open
shape(non closed loop abosrber)
        B = g_absorber(:,i+1);
        PB = B-P;
        C = g_absorber(:,i+2);
        PC = C-P;
        while(CrossProduct(PC,PB)>0);% find the tangent line to be PB
            i=i+1;
            %A = g_absorber(:,i);
            B = g_absorber(:,i+1);

            % check if the absorber is closed, if it is not, the program can
            % run out of points on C. If it is so, C has to be kept as the
last
            % point.
            if(i+2>size(g_absorber,2))
                %PA = A-P;
                PB = B-P;
                PC = C-P;
                break;
            end
            C = g_absorber(:,i+2);
            %PA = A-P;
            PB = B-P;
            PC = C-P;
            %plotLine(A,P);
        end
    end
end
%g_shapeData
xlswrite('CPC.xls',xlsData);
xlswrite('Absorber.xls',absorberExcelData);
arcLength = arcLength*2
```

```
arcToApertureRatio = arcLength/(idealApertureLength*g_truncatingPercentage)
concRatio = 1/sin(g_acceptanceAngle)*g_truncatingPercentage
hightToAperture = (max(g_shapeData(2,:))-
min(g_shapeData(2,:)))/((idealApertureLength*g_truncatingPercentage))
apertureResult = (idealApertureLength*g_truncatingPercentage)
%hard Coded sampling process:
pointNumber = 300;
xlsSampled = [];

if size(g_shapeData,2)>pointNumber
    ratio = floor(size(g_shapeData,2)/pointNumber);
    sampledData = {sprintf('%.3fmm',g_shapeData(1,1)),
sprintf('%.3fmm',g_shapeData(2,1)),'0mm'};
    lastPoint = g_shapeData(:,1);
    for i = 1:ratio:size(g_shapeData,2);
        if (norm(lastPoint-g_shapeData(:,i))>arcLength/pointNumber/8)
            lastPoint = g_shapeData(:,i);
            pointStr = {sprintf('%.3fmm',g_shapeData(1,i)),
sprintf('%.3fmm',g_shapeData(2,i)),'0mm'};
            sampledData = [sampledData;pointStr];
        end;
    end;
    xlswrite('sampledData.xls',sampledData);
else
    display('not enough points to sample');
end
```

## Absorber.m (Examples and V groove gap loss absorber shape)

```
function totalLength = Absorber(shapeNumber)
global g_absorber;
global g_unitLength;
%% starting from the lowest point of the shape up to the highest point, the
shape is symetrical in this case.
%% Note: the shape proposed must be starting from the y axis and end at y
axis;
%
% % %% examples:
totalLength = 0;
g_absorber = [];
switch shapeNumber
    case 1
        %pentagon shape
        radius  =96/2*cos(22.5/180*pi);
        bottomPoint=-102/2-0.5;
        g_absorber = [0;bottomPoint];
        for theta = 2*pi/5+3/2*pi:2*pi/5:(2+.5)*pi
            g_absorber = [g_absorber,[radius*cos(theta);radius*sin(theta)]];
        end

    case 2
        %% minichannel absorber:
        radius = .5;
        g_absorber = [0;0];
        g_absorber = [g_absorber,[radius;2]];
```

```
        g_absorber = [g_absorber,[radius;27]];
        for theta = 0.001:10/180*pi:pi/2-0.001
        g_absorber = [g_absorber,[radius*cos(theta);70/2+radius*sin(theta)]];
        end;

    case 3
        %1.circle with radius being 10;
        radius = 22/2;
        for theta = 3/2*pi:0.5*pi/180:5/2*pi;
            g_absorber = [g_absorber,[radius*cos(theta);radius*sin(theta)] ];
        end

    case 4
        % circular shape with gap consideration
        radius  =96/2*cos(22.5/180*pi);
        bottomPoint=-102/2-1.5;
        g_absorber = [0;bottomPoint];
        angle = acos(radius/(-bottomPoint));
        for theta = -1/2*pi+angle+0.1/180*pi:0.5/180*pi:pi/2
            g_absorber = [g_absorber,[radius*cos(theta);radius*sin(theta)]];
        end;
    case 5
        %58mm absorber icecream cone design
        radius = 6; %% size of the center tube
        g_absorber = [0.12;0];
        for theta = 2*pi-0.3398:1*pi/180:2*pi+pi/2
        g_absorber =
[g_absorber,[radius*cos(theta);radius*sin(theta)+3*radius] ];
        end
    case 6
        %85mm absorber icecream cone design
        radius = 6;
        g_absorber = [0.12;0];
        for theta = 2*pi-0.2026:1*pi/180:2*pi+pi/2
            g_absorber =
[g_absorber,[radius*cos(theta);radius*sin(theta)+32.2950] ];
        end
    case 7
        % hand drawn 1.
        x = [-5,-4.8,-4,-3,0,3,4,4.8,5];
        y = [0,.3,.9,1.2,1.5,1.2,.9,.3,0];
        xx = -5:.25:5;
        yy = spline(x,y,xx);
        g_absorber = [yy;xx];
    case 8
        % hand drawn 2
        x = [-5,0,5];
        y = [0,1,0];
        xx = -5:.25:5;
        yy = spline(x,y,xx);
        g_absorber = [yy;xx];

    case 9
        %3.octangle
        g_absorber = [g_absorber,g_unitLength*[0;-1]];
        g_absorber = [g_absorber,g_unitLength*[2^.5/2;-2^.5/2]];
```

```
        g_absorber = [g_absorber,g_unitLength*[1;0]];
        g_absorber = [g_absorber,g_unitLength*[2^.5/2;2^.5/2]];
        g_absorber = [g_absorber,g_unitLength*[0;1]];

    case 10
        % random points.
        g_absorber = [g_absorber,g_unitLength*[0;-2]];
        g_absorber = [g_absorber,g_unitLength*[1;-1]];
        g_absorber = [g_absorber,g_unitLength*[2;1]];
        g_absorber = [g_absorber,g_unitLength*[2;1.5]];
        g_absorber = [g_absorber,g_unitLength*[0;3]];

    case 11
        % changed absorber
        radius = 6; %% size of the center tube
        g_absorber = [6;0];
        for theta = 0:1*pi/180:pi/2
            g_absorber =
[g_absorber,[radius*cos(theta);radius*sin(theta)+3*radius] ];
        end;
    case 12
        radius  =92/2;
        %square shape
        height = 5+radius;
        g_absorber = [0.001;0];
        g_absorber = [g_absorber,[radius*cos(0);height+radius*sin(0)]];
        g_absorber = [g_absorber,[radius*cos(pi/2-
0.001);height+radius*sin(pi/2-0.001)]];
    case 13
        %flat absorber
        g_absorber = [10;0];
        g_absorber = [g_absorber,[0.1;0]];
    case 14
        %radius  =92/2;
        offset = -2.5;
        %g_absorber = [0.001;-46];
        g_absorber = [0.001;-49+offset];
        %g_absorber = [g_absorber,[2.619;-45.1356]];
        g_absorber = [g_absorber,[44.91805974;9.91805974+offset]];
        g_absorber = [g_absorber,[24.68280878;38.81699307+offset]];
        g_absorber = [g_absorber,[0.001;38.81699307+offset]];
    case 15
        %% oval shape:
        g_absorber = [0;0];

        %g_absorber = [g_absorber,[0;28.2]];
        g_absorber = [g_absorber,[0;(63+4)]];
    case 16
        %% v groove shape
        %inner circle;
        i_radius = 14;
        %outer circle;
        o_radius = i_radius+2;
        %outer circle start point
        theta = (acos(i_radius/o_radius)*180/pi-2)*pi/180;%15 is the angle
starting from the middle line.
```

```
        theta = theta*0.99;
        %theta should be less(a little bit, not increasing fast) than
        if theta>acos(i_radius/o_radius);
            display('warning: starting angle should be less than:');
            acos(i_radius/o_radius)*180/pi;
        end
        start_angle = -pi/2+theta;
        g_absorber =[o_radius*cos(start_angle);o_radius*sin(start_angle)];
        %inner circle starting angle.
        i_start_angle = start_angle +acos(i_radius/o_radius);
        spacing = (pi/2-i_start_angle)/40;
        for step = i_start_angle:spacing:pi/2;
            g_absorber =
[g_absorber ,[i_radius*cos(step);i_radius*sin(step)]];
        end
end



%2.square with weird shape.
% g_absorber = [g_absorber,g_unitLength*[0;-2]];
% g_absorber = [g_absorber,g_unitLength*[1;-1]];
% g_absorber = [g_absorber,g_unitLength*[2;1]];
% g_absorber = [g_absorber,g_unitLength*[2;1.5]];
% g_absorber = [g_absorber,g_unitLength*[0;3]];


%% duplicating the other half.
if(g_absorber(1,end)>=0.00001)% the unequal ~= check does not satisfy,
sometimes it fails below 1e-15.
    for i = size(g_absorber,2):-1:1
        g_absorber = [g_absorber,[-g_absorber(1,i);g_absorber(2,i)] ];
    end
else
    for i = size(g_absorber,2)-1:-1:1
        g_absorber = [g_absorber,[-g_absorber(1,i);g_absorber(2,i)] ];
    end
end
for i=1:size(g_absorber,2)-1
    totalLength=totalLength+norm(g_absorber(:,i)-g_absorber(:,i+1));
end
end
```